Patterning of Polar Active Filaments on a Tense Cylindrical Membrane

Pragya Srivastava,[1] Roie Shlomovitz,[2] Nir S. Gov,[3] and Madan Rao[1,4]

[1]*Raman Research Institute, Bangalore 560080, India*
[2]*Department of Physics, University of Washington, Seattle, Washington 98195, USA*
[3]*Chemical Physics, Weizmann Institute of Science, Rehovot 76100, Israel*
[4]*National Centre for Biological Sciences (TIFR), Bangalore 560065, India*

(Received 9 June 2012; published 18 April 2013)

We study the dynamics and patterning of polar contractile filaments on the surface of a cylindrical cell using active hydrodynamic equations that incorporate couplings between curvature and filament orientation. Cables and rings *spontaneously* emerge as steady state configurations on the cylinder, and can be stationary or moving, helical or tilted segments moving along helical trajectories. We observe phase transitions in the steady state patterns upon changing cell diameter or motor-driven activity and make several testable predictions. Our results are relevant to the dynamics and patterning of a variety of active biopolymers in cylindrical cells.

DOI: 10.1103/PhysRevLett.110.168104 PACS numbers: 87.16.Ka, 87.16.Ln, 87.17.Rt

Cytokinesis, a common mechanism by which cells divide, involves the regulated assembly and constriction of a contractile actomyosin ring. A well studied model system of the dynamics of assembly of the contractile ring is fission yeast (*S. pombe*) [1]. The contractile ring appears to assemble on the inner cell surface via heterogeneous nucleation of nodes and growth of actin cables [1]. Recent experiments on cylindrical fission yeast and its mutants have shown that the stability and dynamics of the contractile ring is greatly influenced by cell geometry [2]. In this Letter, we present a general model that takes into account the interplay between cell geometry and actomyosin activity, which accounts for the various phenotypes exhibited by the actomyosin filaments. Indeed this interplay between geometry and cytoskeletal mechanics has been well appreciated in the context of mitotic division in epithelial cells [3].

We present an extensive analysis of the steady state patterns of active polar filaments (e.g., actomyosin) on the (inner) surface of a nondeformable cylindrical cell, using the equations of active hydrodynamics [4] generalized to include the coupling of geometry to filament orientation [5]. Such nondeformable cylindrical cell surfaces are realized in rod-shaped bacteria and fission yeast cells, due to their strong coupling to a rigid cell wall [1]. While our study complements the approach based on microscopic agent-based simulations [6,7], it has significant points of difference, notably the influence of cell geometry and cell size. Our main results are (a) rings and cables appear as generic steady state patterns, either from a spinodal instability of the homogenous configuration (Figs. 1 and 2) or from a nucleation and growth of an actin node (Fig. 3). Rings or cables may be either stationary or mobile, and their width is set by the curvature-dependent, active Peclét length L_p. (b) Phase transitions between the different steady state configurations can be achieved by changing cell diameter (Fig. 1). (c) Because of the intrinsic anisotropy in the curvature of the cylindrical cell, the active filaments can exhibit helical shapes or tilted segments which move along helical trajectories

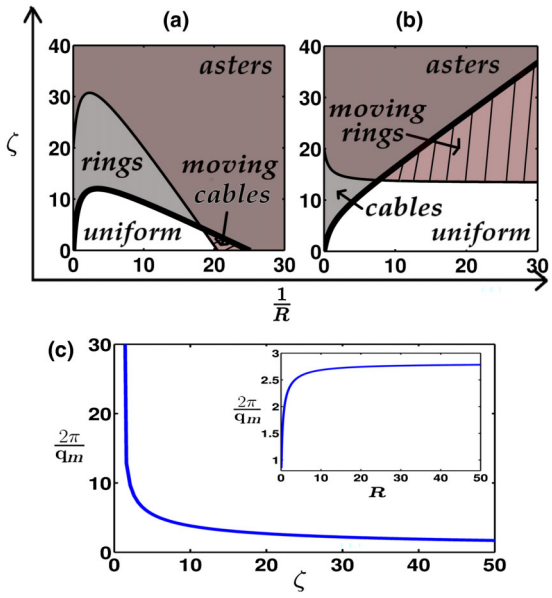

FIG. 1 (color online). Phase diagram in ζ-R at high filament concentration and net mean orientation, obtained from linear stability analysis, for (a) $\alpha_\theta > 0$ and $\alpha_\theta > \alpha_z$ and (b) $\alpha_z > 0$ and $\alpha_z > \alpha_\theta$. The steady state patterns corresponding to these phases are depicted in Fig. 2. Uniform phase refers to homogeneous, oriented phase along (a) $\hat{\theta}$ and (b) $\hat{z}$. The phase boundaries in (a) correspond to $\zeta_{c1} = D(\alpha_\theta - \alpha_z)/c_0 v_z$ (thick line) and $\zeta_{c2} = 2D\alpha_\theta/c_0 v_\theta$ (thin line), and in (b) correspond to $\zeta_{c1} = D(\alpha_z - \alpha_\theta)/c_0 v_\theta$ (thick line) and $\zeta_{c2} = 2D\alpha_z/c_0 v_z$ (thin line). (c) Scaling of the inverse of the fastest growing wave vector q_m with ζ (for fixed $R = 10$) and (inset) with R (for fixed $\zeta = 20$), corresponding to the ring phase in (a). Values of other parameters are as listed in Ref. [11].

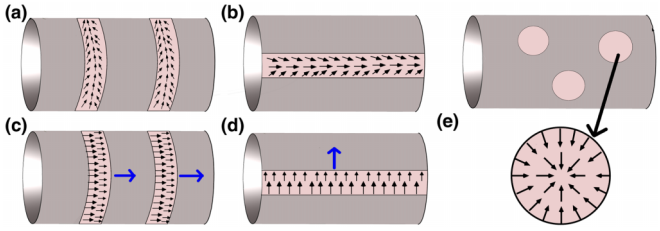

FIG. 2 (color online). Schematic of steady state patterns characterizing the phases in Fig. 1: (a) stationary rings, (b) stationary cables, (c) moving rings, (d) moving cables, (e) asters or nodes. Small arrows (black) show texture and thick arrows (blue) denote direction of movement of the rings or cables.

(Fig. 4). (d) Proximal rings merge to form one ring; the dynamics of ring merger is controlled by activity. In addition to relating some of our results to existing experiments, we make several quantitative predictions which could be experimentally tested.

We describe the dynamics of active polar filaments in a two-dimensional cylindrical surface $\mathcal{S}$, in terms of a local concentration $c(\mathbf{r}, t)$ and polarization $\mathbf{n}(\mathbf{r}, t) = (n_\theta, n_z)$, representing the polar orientation (equivalently, the velocity of the filaments relative to the medium). Assuming that momentum gets dissipated predominantly by friction at the cortex, the hydrodynamic velocity is obtained from local force balance, $\Gamma \mathbf{v} = \nabla \cdot \sigma$, where $\sigma = -Wc\mathbf{nn}$ is active contractile stress with $W < 0$ [8]. When the total number of actin filaments in the cortex is conserved, $\partial_t c = -\nabla \cdot \mathbf{J}$,

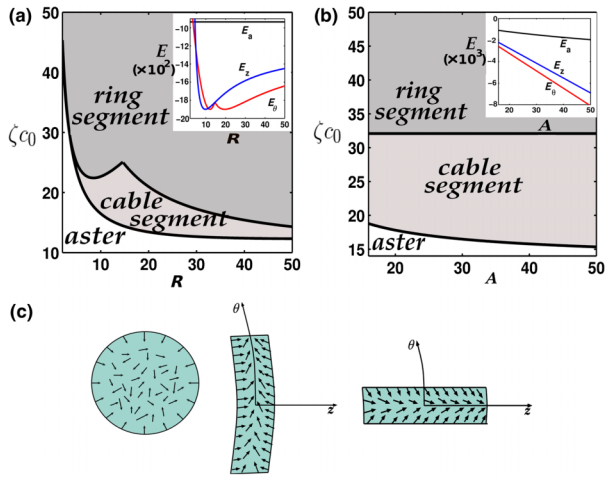

FIG. 3 (color online). Phase diagram in ζc_0 versus (a) R (at constant $A = 30$) and (b) A (at constant $R = 10$) showing asters (nodes), ring segment, and cable segment. Insets show the "energy" branches (units of K) of the three configurations, Eq. (3). The energy branches in the insets have been plotted for (a) $\zeta c_0 = 25$ and (b) $\zeta c_0 = 40$. Note that the form of E_θ in Eq. (3) is valid for a ring segment of width D/v_z, which does not encircle the cylinder. For smaller values of R [below the kink in (a)], the ring segment completely encircles the cylinder, its width is now set by $A/2\pi R$. The orientation of $\mathbf{n}$ in these configurations is shown in (c). All the parameters are in scaled units [11].

where $\nabla \equiv (R^{-1}\partial_\theta, \partial_z)$ is the differential operator on the surface of cylinder of radius R. The filament current $J_i = v_0 c n_i + \Lambda^{kl}_{ij}\kappa^j_k c n_l - D\nabla_i c$, where the first term is an active advection [e.g., motor driven or (de)polymerization] with speed v_0, the second is an anisotropic advection due to coupling between $\mathbf{n}$ and the curvature tensor κ^i_j, and the third is a diffusive current with coefficient D. We will implicitly assume that the filaments are short compared to the cell size.

The dynamics of the polarization $\mathbf{n}$ is obtained by generalizing the Toner-Tu equations [9] to include symmetry allowed couplings to cell geometry,

$$\frac{\partial \mathbf{n}}{\partial t} + \lambda(\mathbf{n}\cdot\nabla)\mathbf{n} = K_1\nabla^2\mathbf{n} + K_2\nabla(\nabla\cdot\mathbf{n}) + \zeta\nabla c + (\alpha - \beta|n|^2)\mathbf{n} + \boldsymbol{\gamma\kappa}\mathbf{n}, \quad (1)$$

where the Laplacian is defined on the surface of the cylinder, and the last term implies tensor contraction. The nonlinear convective term λ is purely active in origin [9], while $K_{1,2}$ are active torques that promote relative alignment of neighboring filaments. The values of α, β are chosen such that $|\mathbf{n}| \approx 1$ almost everywhere.

The 4th rank tensor parameters Λ^{ij}_{kl} and γ^{ij}_{kl} are the most general phenomenological couplings between curvature κ^i_j and polar order $\mathbf{n}$ to lowest order. While the coupling parameter γ^{ij}_{kl} can be present even in an equilibrium membrane with a tilt field [10], the parameter Λ^{ij}_{kl} is purely active in origin. To arrive at the independent components of these tensor parameters, we note that the dynamical equations should be invariant under $\theta \to -\theta$ and $z \to -z$; this together with the form of the curvature tensor for the cylinder

$$\kappa = \begin{pmatrix} 1/R & 0 \\ 0 & 0 \end{pmatrix}$$

immediately implies that only $(\Lambda^{\theta\theta}_{\theta\theta}, \Lambda^{z\theta}_{\theta z})$ and $(\gamma^{\theta\theta}_{\theta\theta}, \gamma^{z\theta}_{\theta z})$, denoted as Λ_i, γ_i with $i = \theta$, z, respectively, are

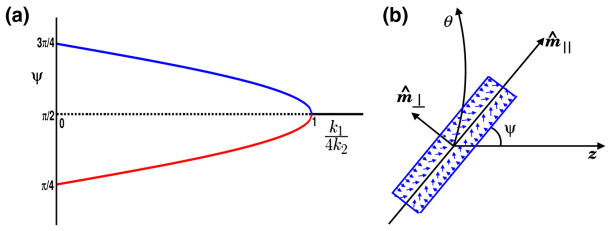

FIG. 4 (color online). (a) Orientation of tilted segment ψ, schematically represented in (b), with (short) arrows showing $\mathbf{n}$ within the segment. The steady state tilt plotted as a function of $k_1/4k_2$ shows a continuous transition from a ring segment ($\psi = \pm\frac{\pi}{2}$) to a tilted segment (see text) at $k_1/4k_2 = 1$. The symmetries of a cylinder allow for four stable solutions: the two shown above have a net orientation of $\mathbf{n}$ along ψ, while two more have a net orientation of $\mathbf{n}$ along $-\psi$.

independent [11]. Note that the Λ_i's trivially renormalize the advection v_0 in the c equation, giving rise to an anisotropic advection $v_i = v_0 + \Lambda_i/R$. Similarly, the γ_i's renormalize the coefficient of the linear term α in Eq. (1) to $\alpha_i = \alpha + \gamma_i/R - \delta_{i\theta}K_1/R^2$, where δ_{ij} is the Kronecker delta. In what follows, we let γ_i have positive and negative values, and restrict $K_{1,2}$ to the positive domain (see discussion).

The parameter α is a linear function of the mean filament concentration c_0 and governs the transition from orientationally disordered to polar ordered phase, while $\zeta > 0$ describes the tendency of contractile filaments to reorient towards the gradient of concentration [12]. Because of activity, the filaments move relative to the solvent in the direction of $\mathbf{n}$; thus, reorientation is accompanied by movement of filaments towards each other (if, $\zeta v_i > 0$) and can, for instance, be enhanced by increasing motor activity. Since the number of parameters is large, we restrict ourselves to parameter ranges which are both representative and accessible to experimental manipulation. We explore the steady state patterns of active filaments on a cylindrical cell as a function of (i) c_0, (ii) ζ, and (iii) cell size R. Values of parameters used correspond to those in fission yeast, and are tabulated in Ref. [11].

Spinodal instability.—We first study the instability of the homogeneous phase when the filament concentration is high, so that one or both of the α's are positive $[\alpha_i(c_0, R) > 0]$ and the homogeneous solution $c = c_0$ has polar order (Fig. 1). The spontaneous polarization $\mathbf{n}_0$ is determined by the largest α and can be along either the azimuthal (θ axis) or the axial (z axis) direction. This homogeneous polar phase becomes linearly unstable to the formation of spatial structures when ζ is increased beyond a threshold. The nature of instability is the same whether $\alpha_\theta > \alpha_z$ or vice versa, and hence we discuss only the former case, where we perturb the system around $\mathbf{n}_0 = \sqrt{\alpha_\theta/\beta}\hat{\theta}$. The orientation of the spatial structure is set by the fastest growing wave vector $\mathbf{q}_m$ of the dispersion surface: (i) when $\zeta_{c2} > \zeta > \zeta_{c1} = \frac{D(\alpha_\theta - \alpha_z)}{c_0 v_z}$, the instability is along $\hat{z}$, while (ii) when $\zeta_{c1} > \zeta > \zeta_{c2} = \frac{2D\alpha_\theta}{c_0 v_\theta}$, the instability is along $\hat{\theta}$. Figure 1(c) shows the dependence of the magnitude of the fastest growing wave vector on R and ζ; the exact expressions are displayed in Ref. [11].

While the onset of instability (phase boundaries) and their nature can be obtained by a linear stability analysis (Fig. 1), the final steady state configurations of c and $\mathbf{n}$ cannot. To ascertain this, we numerically integrate the dynamical equations for c and $\mathbf{n}$ using an implicit and alternating direction method [13]. The finite wave vector instability seen in the linear analysis shows up as a density clumping along a specific direction. For parameter ranges where the real part of the dispersion surface has only one maxima, such as (i) and (ii) above, the direction of the density clumping is set by the direction of the fastest growing wave vector $\mathbf{q}_m$ [11]; thus, when $\mathbf{q}_m$ is along $\hat{z}$, we obtain rings, while when $\mathbf{q}_m$ is along $\hat{\theta}$, we get cables. These rings or cables can be stationary or moving as determined by the imaginary part of the dispersion relations. The steady state orientation $\mathbf{n}$ within the stationary or moving rings or cables, obtained from a numerical solution of the dynamical equations, is shown in Fig. 2. On the other hand, when $\zeta > \max(\zeta_{c2}, \zeta_{c1})$, the dispersion surface has two maxima, one along $\hat{z}$ and the other along $\hat{\theta}$ [11], and a numerical solution of the dynamical equations shows that the steady state configuration is an array of inward-pointing asters or nodes (Fig. 2). For the case when $\alpha_z > 0$ and $\alpha_z > \alpha_\theta$ (i.e., when the spontaneous polarization is along $\hat{z}$), the phase diagram is shown in Fig. 1(b).

The magnitude of $\mathbf{q}_m^{-1}$ corresponds to the periodic separation between rings, as verified from a numerical solution of the equations. This leads to two predictions [Fig. 1(c)]: (i) the separation between rings increases monotonically with R and saturates to a constant which depends on ζ and (ii) for fixed R, the separation decreases with contractility as $1/\sqrt{\zeta}$ (exact expressions for q_m are given in Ref. [11]). These scaling predictions can be tested experimentally.

The width w of the rings and cables (and aster size) is set by the ratio $D/v_{\theta,z}$, the curvature-dependent active Peclét length L_p, which balances diffusion with advection. To obtain the leading contribution to the ring velocity, we use the ansatz for an axisymmetric moving ring $c \equiv c[z - z_0(t)]$ together with the assumption that the other variables, such as w and the polarization profile are fast; integration over the ring area then gives $\dot{z}_0(t) = v_z \equiv v_0 + \Lambda_z/R$. Since $\zeta v_i > 0$, this immediately leads to another prediction of the model; namely, the velocity of the moving ring is higher for narrower cylinders and approaches v_0 as Λ_z/R, when R is large. Similar arguments suggest that the velocity of moving cables is v_θ. These predictions can be tested in experiments such as [14].

Nucleation and growth.—Thus far we have studied the spinodal instability of the uniform phase to coherent structures. In the context of fission yeast, however, actin is nucleated at the cell surface by the actin nucleator *formin* [1], which first forms a node then grows into a ring or cable. We study the transition between these domain shapes [aster → ring or cable segment, Fig. 3(c)] using a variational calculation. Actin nucleation is modeled by a source term in the c equation, which goes to vary the domain area A, assuming that the concentration is uniform at c_0. The aster size is completely fixed by A, while the dimensions of the ring or cable segments are fixed by A and the width; the latter is obtained from current balance and is given by the active Peclét length $D/v_{\theta,z}$. To obtain the texture within the domain $\mathcal{S}$, we note that when $\lambda \to 0$, the steady state solutions of $\mathbf{n}$, Eq. (1), can be obtained as minimizers of an "energy" functional (strictly, Lyapunov functional [15]),

$$E[c,\mathbf{n}] = \int_{\mathcal{S}} [(K_1+K_2)(\nabla\cdot\mathbf{n})^2 + K_1(\nabla\times\mathbf{n})^2 + \zeta c(\nabla\cdot\mathbf{n})], \tag{2}$$

together with a local constraint on the magnitude, $\mathbf{n}\cdot\mathbf{n} \equiv n_0^2 = \alpha_{\theta,z}/\beta$. Finally, we compare the "energies" of the inward aster (E_a), ring segment (E_θ), and cable segment (E_z) with the same area A and mean concentration c_0, in a one constant approximation, $K_1 = K_2 = K$,

$$\begin{aligned} E_a &= \pi K \ln\frac{A}{\pi\xi^2} - 4\pi\zeta c_0\sqrt{\frac{A}{\pi}} + \epsilon_c, \\ E_{\theta,z} &= \left[\frac{\pi^2 K}{D^2}\left(v_0 + \frac{\Lambda_{z,\theta}}{R}\right)^2 - \frac{2\zeta c_0}{D}\left(v_0 + \frac{\Lambda_{z,\theta}}{R}\right)\right]A, \end{aligned} \tag{3}$$

where ξ and ϵ_c are the core size and energy, respectively. Note that E_a is the same as in a planar geometry, since the Gaussian curvature of a cylinder is zero [16]. The energy branches and the phase diagram are shown in Fig. 3; a typical nucleation and growth scenario would correspond to a trajectory in the $(\zeta c_0, A)$ plane and shows the transition between node $\rightarrow$ cable segment $\rightarrow$ ring segment seen in experiments [14].

Thus far, the steady state configurations correspond to rings (cables) along the θ (z) axis alone; no other orientation is permitted. However, in principle, the parameters accompanying the nonlocal terms in (1), namely, K_1, K_2, and ζ, can also have anisotropies consistent with cylindrical symmetry. This could arise, for instance, from having "easy directions" [17] for spatial variations of $\mathbf{n}$ and c.

Consider a tilted segment at an angle ψ to the cylinder axis, $\psi = \cos^{-1}(\hat{\mathbf{m}}_\parallel\cdot\hat{\mathbf{z}})$, where $\hat{\mathbf{m}}_\parallel$ is the unit vector along the segment boundary, Fig. 4(b), having a uniform width $w(\psi)$ and length $l(\psi)$ such that the area $A = wl$ is fixed. For simplicity, we assume that within the tilted segment, the filament concentration $c = c_0$ is uniform. The texture within the tilted segment is shown in Fig. 4(b), the orientation of $\mathbf{n}$ changes by π on a length scale $w(\psi)$. The width of the tilted segment $w(\psi)$ is set by a balance of the net current $\mathbf{J}\cdot\hat{\mathbf{m}}_\perp$, where $\hat{\mathbf{m}}_\perp$ is a unit vector normal to the boundary. In the equal constants approximation, $K_1 = K_2 = K$, the energy (2) of this tilted segment is given by

$$E(\psi) = K(\psi)\frac{\pi^2 A}{w(\psi)^2} - 2\zeta(\psi)c_0\frac{A}{w(\psi)}, \tag{4}$$

and the steady state orientation of the tilted segment is obtained by setting $\frac{\partial E}{\partial\psi}|_A = 0$. To prove our point, it suffices to look at the anisotropy of $K(\psi)$ alone, which, owing to cylindrical symmetry, can be written as $K(\psi) = \sum_m k_m \cos 2m\psi$, of which we take only the first two modes. The phase diagram Fig. 4 shows a continuous transition from a ring segment with $\psi = \pm\pi/2$ to a tilted segment with $\psi = \cos^{-1}\sqrt{\frac{1}{2}(1-\frac{k_1}{4k_2})}$, as $k_1/4k_2$ is varied. Because the net polarization of these *active* tilted segments is along ψ, short segments will appear to *move* on helical tracks. On the other hand, longer tilted segments will appear as moving helices. These results are relevant to recent observations on the movement of MreB filaments on helical tracks, whose strong anchoring to the cell wall growth machinery provides the easy directions on the surface of these rod-shaped bacteria [18], and on propagating helices of FtsZ in *B. subtilis* [19,20].

We end with a discussion on the fate of multiple rings, both moving and stationary. Well separated rings moving along the $+z$ axis result in periodic oscillations in time (with a time period $\tau = L/v_z$, which gets smaller for narrower cylinders), when we impose no flux boundary conditions along z or when the cylinder is capped on either end by hemispheres. On the other hand, stationary rings, proximal to each other, merge to eventually form a single ring whose width is the same as the original rings, as observed in experiments on reconstituted cylindrical liposomes [21].

Discussion.—In summary, we have presented a detailed analysis of the effect of curvature-orientation coupling on the patterning of active filaments in a cylindrical cell and predict a rich variety of steady state patterns which include asters (nodes) and stationary and moving rings and cables. Our work is valid in those situations where we can ignore the deformation of the cell membrane, which can itself contribute to additional instabilities [22]. We have implicitly assumed that $K_{1,2} \geq 0$, thus obtaining parallel filament orientations within the ring. However, the steady states also admit antiparallel filament orientations [23] if $K_{1,2} < 0$; one then needs to augment Eq. (1) by a symmetry allowed fourth-order spatial derivative for stability. The coarse-grained symmetry-based approach presented here is complementary to the more microscopic agent-based simulations, and has the advantage of being applicable to a variety of cellular contexts such as (i) actin filaments in fission yeast cells [1], (ii) reconstituted cytoskeletal elements on cylindrical liposomes [21], (iii) FtsZ filaments in bacteria (and reconstituted in yeast [24]), and (iv) MreB filaments in rod-shaped bacteria [18]. A more detailed comparison to experiments will be taken up later. Our work sets the stage to study the dynamics of quenches from one phase to another, which is appropriate to the study of the growth of cables or rings from the nucleation of nodes of actomyosin filaments in fission yeast [25,26].

We thank M. Balasubramanian and his group for discussions and collaborations. M. R. thanks HFSP and N. S. G. thanks the Minerva Foundation for support (Grant No. 710589).

[1] T. D. Pollard and J. Q. Wu, Nat. Rev. Mol. Cell Biol. **11**, 149 (2010).
[2] M. Mishra, Y. Huang, P. Srivastava, R. Srinivasan, M. Sevugan, R. Shlomovitz, N. Gov, M. Rao, and M. Balasubramanian, J. Cell Sci. **125**, 3850 (2012).

[3] D. Odde, Cell **144**, 325 (2011).
[4] M. C. Marchetti, J. F. Joanny, S. Ramaswamy, T. B. Liverpool, J. Prost, M. Rao, and R. A. Simha, arXiv:1207.2929.
[5] Similar questions have been addressed in A. Zumdieck, M. Lagomarsino, C. Tanase, K. Kruse, B. Mulder, M. Dogterom, and F. Jülicher, Phys. Rev. Lett. **95**, 258103 (2005); however their model for *apolar* order is one dimensional and hence does not include the effects of curvature or cell diameter.
[6] D. Vavylonis, B. Shaughnessay, and T. Pollard, Science **319**, 97 (2008).
[7] N. Ojkic and D. Vavylonis, Phys. Rev. Lett. **105**, 048102 (2010).
[8] Y. Hatwalne, S. Ramaswamy, M. Rao, and R. A. Simha, Phys. Rev. Lett. **92**, 118101 (2004).
[9] J. Toner and Y. H. Tu, Phys. Rev. E **58**, 4828 (1998).
[10] R. C. Sarasij and M. Rao, Phys. Rev. Lett. **88**, 088101 (2002).
[11] See Supplemental Material at http://link.aps.org/supplemental/10.1103/PhysRevLett.110.168104 for symmetry arguments for curvature orientation coupling, a table with the values of parameters in real and scaled units, the numerical scheme, exact dispersion relations, and phase diagrams.
[12] K. Gowrishankar and M. Rao, arXiv:1201.3938.
[13] W. H. Press, B. P. Flannery, S. A. Teukolsky, and W. T. Vetterling, *Numerical Recipes in Fortran: The Art of Scientific Computing* (Cambridge University Press, Cambridge, England, 1999).
[14] J. Huang, Y. Huang, H. Yu, D. Subramanian, A. Padmanabhan, R. Thadani, Y. Tao, X. Tang, R. Wedlich-Soldner, and M. K. Balasubramanian, J. Cell Biol. **199**, 831 (2012).
[15] A. J. Bray, Adv. Phys. **51**, 481 (2002).
[16] A. M. Turner, V. Vitelli, and D. R. Nelson, Rev. Mod. Phys. **82**, 1301 (2010).
[17] See Table IV in M. E. Fisher, Rev. Mod. Phys. **46**, 597 (1974).
[18] E. C. Garner, R. Bernard, W. Wang, X. Zhuang, D. Z. Rudner, and T. Mitchison, Science **333**, 222 (2011); J. D. Escobar, A. Chastanet, A. H. Crevenna, V. Fromion, R. Wedlich-Soldner, and R. Carballido-Lopez, Science **333**, 225 (2011).
[19] S. B. Yehuda and R. Losick, Cell **109**, 257 (2002).
[20] E. F. Friedrich, B. M. Friedrich, and N. S. Gov, Phys. Biol. **9**, 016009 (2012).
[21] M. Osawa, D. E. Anderson, and H. P. Erickson, Science **320**, 792 (2008).
[22] R. Shlomovitz and N. S. Gov, Biophys. J. **94**, 1155 (2008); Phys. Biol. **6**, 046017 (2009).
[23] T. Kamasaki, M. Osumi, and I. Mabuchi, J. Cell Biol. **178**, 765 (2007).
[24] R. Srinivasan, M. Mishra, L. Wu, Z. Yin, and M. K. Balasubramanian, Genes Dev. **22**, 1741 (2008).
[25] J. Q. Wu and T. D. Pollard, Science **310**, 310 (2005).
[26] T. Drake and D. Vavylonis, HFSP J. **4**, 122 (2010).